Engineering 20 (2023) 49–62

Contents lists available at ScienceDirect

Engineering

journal homepage: www.elsevier.com/locate/eng

Research
Glucose and Lipid Metabolism—Article

CPAL, as a New Mediator of Cardiomyocyte Metabolic Alterations and Pyroptosis, Regulates Myocardial Infarction Injury in Mice

Jiamin Li [a,c,d,#], Hongru Xue [a,#], Ning Xu [a,#], Liling Gong [a], Ming Li [a], Sijia Li [a], Di Huang [a], Qingwei Zhang [a], Pengyu Li [a], Qingsui Li [a], Hang Yu [a], Yining Liu [a,b], Yadong Xue [a], Haixin Chen [a], Jiali Liu [a], Wanyu Zhang [a], Mingbin Liu [a], Siyu Chang [a], Xianzhi Lang [a], Xingmiao Zhao [a], Weijie Du [a,c,d], Benzhi Cai [b,c,d], Ning Wang [a,c,d,*], Baofeng Yang [a,c,d,*]

[a] State-Province Key Laboratories of Biomedicine-Pharmaceutics of China & Key Laboratory of Cardiovascular Medicine Research (Ministry of Education of the People's Republic of China), Department of Pharmacology, College of Pharmacy, Harbin Medical University, Harbin 150081, China
[b] Institute of Clinical Pharmacy, The University Key Laboratory of Drug Research, Heilongjiang Higher Education Institutions, Department of Pharmacy, the Second Affiliated Hospital of Harbin Medical University, Harbin 150081, China
[c] Research Unit of Noninfectious Chronic Diseases in Frigid Zones (2019RU070), Chinese Academy of Medical Sciences, Harbin 150081, China
[d] Northern Translational Medicine Research and Cooperation Center, Heilongjiang Academy of Medical Sciences, Harbin Medical University, Harbin 150081, China

ARTICLE INFO

Article history:
Received 22 February 2022
Revised 21 July 2022
Accepted 4 August 2022
Available online 14 October 2022

Keywords:
Myocardial infarction
Pyroptosis
CPAL
NFκB
Inflammation

ABSTRACT

Myocardial infarction (MI), the most serious of the ischemic heart diseases, is accompanied by myocardial metabolic disorders and the loss of cardiomyocytes. Increasing evidence has shown that long noncoding RNAs (lncRNAs) are involved in various pathological conditions such as cancer and cardiovascular diseases (CVDs), and are emerging as a novel biomarker for these disorders. This study aims to investigate the regulatory role and mechanisms of lncRNAs in myocardial remodeling in the setting of MI. We find that post-infarcted hearts exhibit a reduction of adenosine triphosphate (ATP) and an alteration of the glucose and lipid metabolism genes cluster of differentiation 36 (CD36), hexokinase 1 (*HK1*), and glucose transporter 4 (*GLUT4*), accompanied by cardiomyocyte pyroptosis. We then identify a previously unknown conserved lncRNA, AK009126 (cardiomyocyte pyroptosis-associated lncRNA, CPAL), which is remarkably upregulated in the myocardial border zone of MI mice. Importantly, the adeno-associated virus 9 (AAV9)-mediated silencing of endogenous CPAL by its short hairpin RNA (shRNA) partially abrogates myocardial metabolic alterations and cardiomyocyte pyroptosis during MI in mice. Mechanistically, CPAL is shown to bind directly to nuclear factor kappa B (NFκB) and to act as an activator of NFκB to induce NFκB phosphorylation in cardiomyocytes. We also find that CPAL upregulates caspase-1 expression at the transcriptional level and consequently promotes the release of interleukin (IL)-18 and IL-1β from cardiomyocytes. Collectively, our findings reveal the conserved lncRNA CPAL as a new regulator of cardiac metabolic abnormalities and cardiomyocyte pyroptosis in the setting of MI and suggest CPAL as a new therapeutic target to protect cardiomyocytes against ischemic injury in infarcted hearts.

1. Introduction

Cardiovascular diseases (CVDs) are a series of congenital or acquired disorders of the heart and blood vessels. At present, CVDs account for more than 40% of all patient deaths in clinics, are a major cause of human death worldwide, and give rise to economic burdens and immense health problems across the globe [1–3]. Myocardial infarction (MI) is one of the most common CVDs; it is a metabolic catastrophe caused by a reduced supply of oxygen and nutrients, which results in microenvironment homeostasis disorder, massive cell death, inflammatory cell infiltration, fibroblast activation, and so forth. These pathological alterations in MI lead to cardiac systolic dysfunction, heart remodeling, myocardial fibrosis, and even sudden cardiac death [4].

Long noncoding RNAs (lncRNAs) are a set of noncoding RNAs that are more than 200 nucleotides (nt) long [5]; they participate

* Corresponding authors.
E-mail addresses: wangning@ems.hrbmu.edu.cn (N. Wang), yangbf@ems.hrbmu.edu.cn (B. Yang).
[#] These authors contributed equally to this work.

https://doi.org/10.1016/j.eng.2022.08.012

in many fundamental pathophysiological processes and biological processes, including genomic imprinting, RNA alternative splicing, and chromatin modification [6]. Numerous studies have shown the differential expression profile of lncRNAs in a variety of CVDs, such as hypertrophy, arrhythmias, and cardiac fibrosis. The knockout of Triadin (Trdn), a cardiomyocyte-specific lncRNA, has been shown to impair the cardiac calcium handling system and increase the susceptibility to cardiac arrhythmias in mice [7]. In addition, a growing number of lncRNAs have been found to participate in the pathological process of MI [8–10]. For example, lncRNA zinc finger antisense 1 (ZFAS1) has been shown to act as a SR Ca2+ATPase 2a (SERCA2a) inhibitor and cause contractile dysfunction by binding to SERCA2a protein in MI mice [11]. It has been reported that lncRNA Krüppel-like factor 3 antisense RNA 1 (KLF3-AS1) plays a potential role in the cardiomyocyte pyroptosis process during the development of MI [12]. The essential roles of lncRNAs in regulating cardiomyocyte death and myocardium remodeling indicate their potential application as new targets for the treatment of MI in the future.

An increasing body of evidence has revealed that MI is accompanied by changes in the cardiac energy metabolism and a massive loss of cardiomyocytes. In particular, impairment in energy and substrate utilization (e.g., glucose and fatty acids (FAs)) has been reported as a key determinant of cell death and myocardial injury in the setting of MI [13,14]. In addition, the continued upregulation of nonspecific indicators of inflammation (e.g., the high-sensitivity interleukin (IL) family) in plasma and the myocardium is associated with worse outcomes. Thus far, some transcription factors, cytokines, enzymes, and growth factors have been shown to be involved in the above mentioned pathological process. Nuclear factor kappa B (NFκB) is a key transcription factor that regulates gene expression in many pathophysiological processes and operates the nuclear translocation of cytoplasmic complexes [15]. It has been reported that quinazoline-4,6-diamine (QNZ) improves glucose uptake through glucose transporter 4 (GLUT4) activation and inhibits chondrocyte degeneration by inhibiting NFκB activation [16]. In addition, NFκB serves as an upstream signal to influence the cardiomyocyte pyroptosis process in the development of MI [17]. The evidence suggests that NFκB plays a crucial role in regulating the functions of vascular endothelial cells and myocardial cells during MI [18,19].

The present study was therefore conducted to explore the function and regulation mechanism of the conserved lncRNA, cardiomyocyte pyroptosis-associated lncRNA (CPAL), in myocardial energy metabolism disorder and inflammatory cardiomyocyte death. Here, we first report that lncRNA CPAL was upregulated in the MI model and induced a reduction of adenosine triphosphate (ATP), alteration of the glucose and lipid metabolism genes cluster of differentiation 36 (*CD36*), hexokinase1 (*HK1*), and *GLUT4*, and myocardial inflammation, which promoted cardiomyocyte pyroptosis and myocardial dysfunction. We further found that NFκB was related to the energy metabolism and inflammatory process of cardiomyocytes in MI. NFκB was phosphorylated by CPAL; the phosphorylated NFκB (P-NFκB) was then transported from the cytoplasm into the nucleus, where it promoted procaspase-1 transcription and activation and led to pyroptosis. This research suggests CPAL as a new regulator and therapeutic target of cardiac metabolic dysfunction and cardiomyocyte pyroptosis in MI.

2. Materials and methods

2.1. Animals

Male C57BL/6 mice weighing 20–25 g were purchased from the Experimental Animal Center of the Affiliated Second Hospital of Harbin Medical University (China). Healthy mice were housed in standard animal room conditions, as previously described [20]. AAV9-ZsGreen-shRNA-NC (AAV9-sh-NC) and AAV9-ZsGreen-shRNA-CPAL (AAV9-sh-CPAL) were delivered into the mouse via tail vein injection; then, four weeks later, the mice were anesthetized with 2,2,2-tribromoethanol (T48402; Sigma–Aldrich, USA) by intraperitoneal injection and were ventilated with a small animal ventilator (model VFA-23-BV; Kent Scientific, USA). The chests were opened between the third and fourth ribs to expose the hearts. A 7-0 nylon sutures were used to ligate around the left coronary artery (LAD); then, the chest was closed [21]. Twenty-four hours after the operation, the hearts were collected for further analyses. Male mice were randomly divided into four groups: the sham group, MI group, +AAV9-sh-NC group, and +AAV9-sh-CPAL group. This study was approved by the Animal Care and Use Committee of Harbin Medical University.

2.2. Construction of CPAL knockdown virus

AAV9 vectors carrying shRNA for silencing CPAL were constructed using a target sequence of 5′-AAACATTAACGAATTAA GACC-3′ and a CAG promoter conjugated with ZsGreen (Hanbio, China). Each mouse was given a titer of 1×10^{12} vg·mL^{-1}(100 μL) via the tail vein [22].

2.3. Echocardiography

2,2,2-Tribromoethanol (T4802; Sigma–Aldrich) was used to anesthetize the mice by intraperitoneal injection. To maintain the body temperature at 37 °C, the mice were positioned on a warming pad. Then, the left ventricular function was evaluated by transthoracic echocardiography, as previously described [4].

2.4. Triphenyltetrazolium chloride (TTC) staining

The mice hearts from each group were excised and frozen rapidly at –80 °C; they were then cut into slices 2 mm thick and stained with 1% TTC in phosphate solution (Sigma–Aldrich, USA) for 20 min at 37 °C. Next, these slices were arranged and digitally photographed.

2.5. Cell culture and treatment or transfection with small interfering RNA (siRNA)

Cardiomyocytes were isolated from neonatal mice (1–3 days old). In brief, the neonatal mice were washed with 75% alcohol; then, a pair of sterile forceps was used to retrieve the hearts. Next, the ventricular myocardium were cut into small pieces. The resulting cell suspension was centrifuged and re-suspended in cell medium with 100 μg·mL^{-1} of streptomycin, 100 U·mL^{-1} of penicillin, and 10% fetal bovine serum. To separate the fibroblasts from the cardiomyocytes, the suspension was placed in culture flasks at 37 °C for 1.5 h. The unattached cells were cardiomyocytes; these were seeded into a cell culture flask and cultured at 37 °C in humid air with 5% carbon dioxide (CO_2). After 48 h, the cardiomyocytes that attached to the culture plates were used for subsequent experiments [23]. The cells were pretreated with/without 5 μg·mL^{-1} of SN50 (HY-P015; MCE, USA) and 50 μg·mL^{-1} of acetyl(Ac)-Tyr-Val-Ala-Asp-chloromethyl ketone (Ac-YVAD-CMK) (178603-78-6; Cayman, USA) for 30 min prior to lipopolysaccharide (LPS) stimulation (50 μmol·L^{-1}, 12 h).

The CPAL-specific siRNA (si-CPAL) and a scrambled negative control RNA (si-NC) were commercially synthesized by GenePharma. The sequences for CPAL were as follows: sense 5′-GGUCUUAAUUCGUUAAUGUTT-3′ and antisense 5′-ACAUUAAC-GAAUUAAGACCTT-3′. The CPAL-specific siRNA was coated and

transfected into cardiomyocytes using Lipofectamine 2000 (Invitrogen, USA) reagent, as described previously [24], with a final concentration of 100 nmol·L^{-1}. At 48 h after transfection, the cells could be used for subsequent experiments.

2.6. Hematoxylin-Eosin (H&E) staining

The hearts of each group mice were dissected and immersed, fixed with 4% paraformaldehyde for 24 h, embedded in paraffin, and then cut into 5-μm-thick sections using tissue-processing equipment. These sections were deparaffinized with xylene and then hydrated with descending concentrations of ethanol. These sections were then stained with a H&E staining kit (G1120; Solarbio, China) according to the manufacturer's protocols, and images were captured by microscopy (FV300, Olympus, Japan).

2.7. Transmission electron microscopy

Cardiomyocytes that had been digested with 0.25% trypsin at 37 °C for 1 min and heart tissues of each group were fixed in 2.5% glutaraldehyde, postfixed in 1% OsO_4 for 2 h, and stained in a block with 1% uranyl acetate, followed by hydration with descending concentrations of ethanol and embedding in epoxy. After electron staining, the sections were observed under electron microscope (JEM-1200; JEOL Ltd., Tokyo, Japan).

2.8. dUTP nick-end labeling (TUNEL) assay

TUNEL staining was used to determine the DNA fragmentation of the cardiomyocytes using a TUNEL detection kit (Roche, Germany) according to the manufacturer's protocol, as previously described [25].

2.9. Western blot

The total protein extraction was based on a bicinchoninic acid (BCA) protein kit (P0012; Beyotime, China) [26]. Protein samples were separated by sodium dodecyl-sulfate polyacrylamide gel electrophoresis (SDS-PAGE; 10%–13%), transferred onto nitrocellulose membranes, and blocked in phosphate-buffered saline (PBS) containing 5% milk. The membranes were then incubated with primary antibodies against nucleotide-binding oligomerization segment-like receptor family 3 (NLRP3) (A12694; Abclonal, USA), Gasdermin D/Gasdermin D N-terminal (GSDMD/GSDMD-N) (ab209845; Abcam, UK), IL-18 (A1115; Abclonal), IL-1β (A16288; Abclonal), caspase-1 (ab207802; Abcam), phospho-nuclear factor kappa B (P-NFκB P65) (Ser536; #3033; CST, USA), NFκB P65 (#8242T; CST), CD36 (74002S; CST), GLUT4 (AF5386; Affinity Biosciences, USA), and HK1 (19662-1-AP; Proteintech, USA) at 4 °C overnight. After washing with PBS with Tween-20 (PBST), the membranes were incubated with fluorescence-conjugated anti-rabbit IgG secondary antibody at room temperature for 1 h (LI-COR, USA). Glyceraldehyde-3-phosphate dehydrogenase (GAPDH) (Zhongshanjinqiao Biological Technology Co., Ltd., China) was used as an internal control. The membranes were scanned and analyzed using an Odyssey Infrared Imaging System (LI-COR).

2.10. Enzyme-linked immunosorbent assay

Enzyme-linked immunosorbent assay (ELISA) kits was used to detect the levels of IL-18 (Elabscience, China), IL-1β (Elabscience), and ATP (MB-6783A; Enzyme Mark Biological, China) in serum, according to the manufacturer's specifications.

2.11. Quantitative real-time polymerase chain reaction (qRT-PCR)

To perform qRT-PCR testing, TRIzol reagent (Invitrogen) was used to extract RNA from the myocardial tissue and cardiomyocytes, as previously described [27]. The complementary DNA (cDNA) synthesis reaction mixture contained 1 μg of the template RNA and the reagents from a high-capacity cDNA reverse transcription kit, according to the instructions. The content of CPAL, NLRP3, caspase-1, IL-18, IL-1β, HK1, and CD36 were detected using a SYBR Green PCR Master Mix kit (Toyobo Co., Ltd., Japan). The relative fold changes were calculated with the $2^{-\Delta\Delta C_t}$ method in the transcripts, which were normalized to endogenous GAPDH levels. The sequences of the primers (mouse) were synthesized by Invitrogen and are shown in Table S1 in Appendix A.

2.12. Immunohistochemical analysis

The heart tissues were fixed, dehydrated, embedded, and sectioned according to standard procedures. Next, these sections were deparaffinized, rehydrated, and blocked with hydrogen peroxide, and then incubated with NLRP3 (BA3677; BOSTER, China), caspase-1 (ab207802; Abcam), and P-NFκB (AF2006; Affinity Biosciences, USA) antibodies at 4 °C overnight. After three washes with PBST, the secondary antibody (Zhongshanjinqiao Biological Technology Co., Ltd.) was used to incubate the slices. The 3,3-*N*-diaminobenzidine tertrahydrochloride (DAB) (Zhongshanjinqiao Biological Technology Co., Ltd.) chromogen was used to incubate the sections, and Mayer's hematoxylin was ultimately used to counterstain the sections in order to stain the cell nuclei. The sections were then photographed under a microscope. ImageJ was used to determine the sizes of the stained areas [28].

2.13. Immunofluorescence

Immunofluorescence staining was used to detect the expression and location of NLRP3, caspase-1, and P-NFκB in the cardiomyocytes. The method used for fluorescence staining was based on a previous description [20]. The following primary antibodies were used: NLRP3 (BA3677; Boster), caspase-1 (ab207802; Abcam), and P-NFκB (AF2006; Affinity Biosciences).

2.14. *Fluorescence* in situ *hybridization*

CPAL expression and localization in cardiomyocytes was evaluated by fluorescence *in situ* hybridization (FISH). In brief, after the cells were cultured to 60%–80% confluences, they were blocked with prehybridization and then permeabilized with 0.5% Triton X-100. After washing and fixing by PBS, the cardiomyocytes were incubated with Cy3-conjugated CPAL probe and 18S and U6 probe in a hybridization buffer. After being washed with saline sodium citrate (SSC) and PBS, the cell nuclei were stained with 4',6-diamidino-2-phenylindole (DAPI). Immunofluorescence was analyzed under a confocal microscope (Axio Scope A1, ZEISS, Germany).

2.15. Chromatin immunoprecipitation (ChIP) assay

The experiment was performed with a chip kit (Invitrogen) according to the instructions. In short, the DNA immunoprecipitated with NFκB P65 antibody and immunoglobulin G (IgG) antibody was detected using polymerase chain reaction (PCR) technology. The following primers were used: *Caspase-1-1* primers (forward 5′-AAAGAAGCCAAGAGCCAGGT-3′ and reverse 5′-AGTGGACCAAGGAATGGTTG-3′) flanked the NFκB binding sites (–836 to –846 nt), and *Caspase-1-2* primers (forward 5′-TGTTTGGTTGGCTGGTTGTT-3′ and reverse 5′-GGACCAGAA-

GCAGAGGTGTG-3′) flanked the NFκB binding sites (−1555 to −1544 nt).

2.16. RNA-interacting protein immunoprecipitation (RIP)

An RIP assay was performed using the MagnaRIP RNA-Binding Protein Immunoprecipitation Kit (17-701; Millipore, Germany), according to the instructions [11]. In brief, heart tissues were harvested and lysed with RIP lysis buffer. Then, the extracted total RNA was mixed with NFκB P65 (622604; Biolegend, USA) antibody or the control antibody (IgG) and precipitated. Next, the precipitated RNA was purified by proteinase K treatment. Finally, the RNA was detected by qRT-PCR.

2.17. The lactate dehydrogenase (LDH) release assay

The LDH release in cells was assessed using an LDH Assay Kit (A020-2, Nanjing Jiancheng Biological, China) according to the manufacturer's instructions.

2.18. Statistical analysis

A statistical analysis of the experimental data was performed using Graphpad Prism 5.0 software (GraphPad Software, Inc., USA). A comparison between the two groups was performed using a *t*-test. One-way analysis of variance (ANOVA) was used to compare multiple groups. Group data are presented as the mean ± the standard error of the mean (SEM), and *P* values of less than 0.05 were considered to be statistically significant.

3. Results

3.1. Myocardial remodeling and alteration of myocardial energy metabolism during MI

First, to reveal the multiple pathological changes associated with cardiac injury in infarcted hearts, we established an *in vivo* MI model by LAD ligation. Echocardiography and hemodynamic measurements showed that ejection fraction (EF) and fractional shortening (FS) were both markedly reduced in the MI heart compared with those in the sham group (Fig. 1(a)). H&E staining of the mouse hearts presented clear structural abnormalities, including changes in the myocardial cell size and the larger intercellular space, accompanied by inflammatory cell infiltration (Fig. 1(b)). Electron microscopy images showed that the basic structure of the myocardium was abnormal in the MI hearts, with swollen mitochondria and karyopyknosis (Fig. 1(c)). In addition, in order to investigate alterations in the myocardial energy metabolism, such as alterations in ATP, glucose, and FAs, their levels were examined during myocardial ischemia. As the main form of energy in the myocardium, ATP can be utilized after MI. Using an ELISA, we found that the ATP level was reduced in the border zone of the infarcted hearts (Fig. 1(d)). The expression of GLUT4, HK1, and CD36 at the mRNA and protein level was visibly downregulated in the MI group (Figs. 1(e) and (f)). These results indicated that the heart injury was increased to varying degrees and might be associated with metabolic alterations and inflammation in MI mice.

3.2. Cardiomyocyte pyroptosis detected in MI hearts

A growing body of evidence has shown that pyroptosis plays a pivotal role in the inflammatory process of MI [29,30]. In the

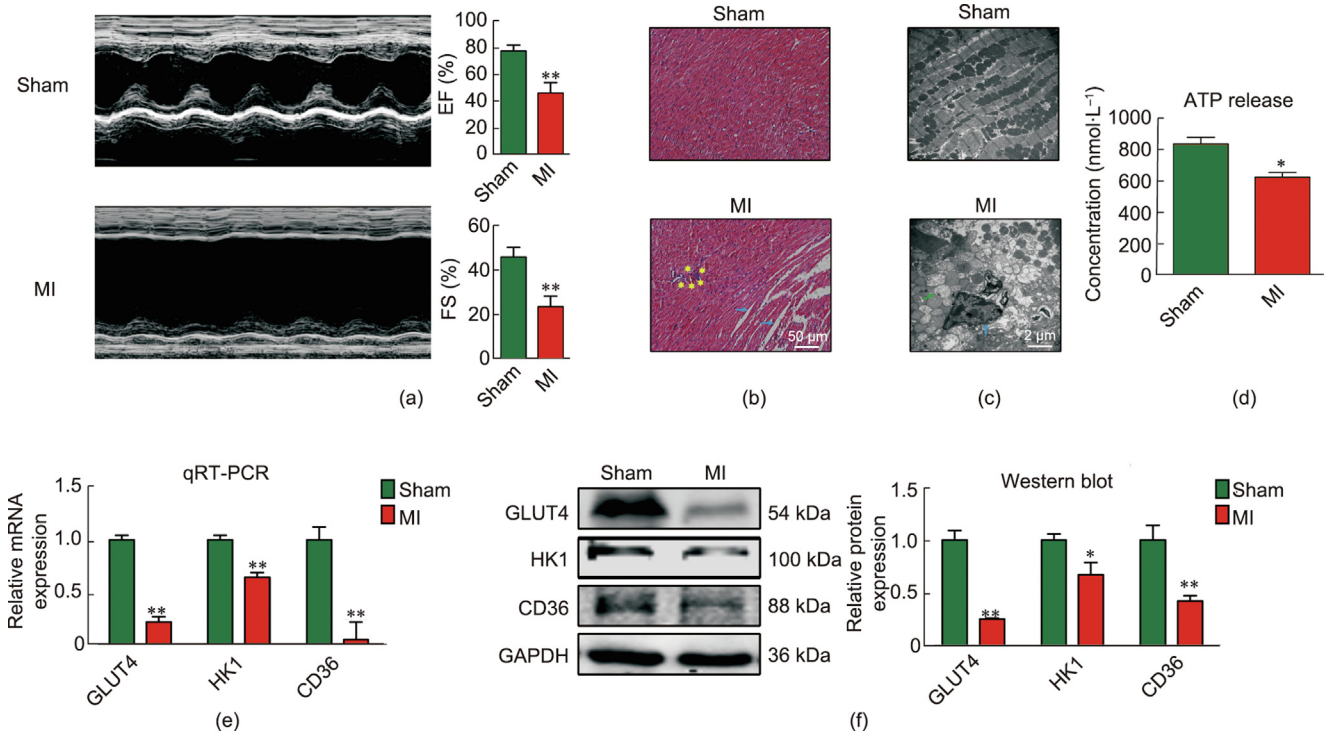

Fig. 1. Heart damage in MI mice. (a) Echocardiogram, EF, and FS measurements of sham and MI mice (n = 5). $^{**}P < 0.01$, compared with sham, mean ± SEM. (b) H&E staining of cross-sectional slices derived from sham and MI hearts (n = 3). The blue arrow indicates the larger intercellular space, and the yellow stars indicate inflammatory cell infiltration. (c) Representative transmission electron microscopy (TEM) micrograph of sham and MI hearts; the blue arrow indicates karyopyknosis, and the green arrow indicates mitochondrial swelling (n = 4). (d) ATP levels in the homogenate of heart tissue from sham and MI (n = 3; $^{*}P < 0.05$). (e, f) The expression of GLUT4, HK1, and CD36 at the mRNA and protein levels in the infarct border zones of the left ventricular from each group at 24 h after the MI operation, respectively ($^{*}P < 0.05$, $^{**}P < 0.01$, compared with the sham group; n = 3 to n = 4; mean ± SEM).

canonical pyroptosis signaling pathway, the oligomerization of pro-caspase-1 proteins guides autoproteolytic cleavage into cleaved caspase-1, then actives the cleavage of GSDMD and induces the release of the GSDMD-N-terminal fragment, which causes membrane pores to release IL-18 and IL-1β with biological activity [28]. To further investigate the degree of inflammatory cell death after MI, a TUNEL staining analysis was performed to determine the DNA integrity in the mouse hearts; it showed numerous TUNEL-positive cells in the MI mouse hearts (Fig. 2(a)). The qRT-PCR results showed that the expression of NLRP3, caspase-1, IL-18, and IL-1β was observably increased at the mRNA level in the MI group (Fig. 2(b)). The protein expression of NLRP3, cleaved caspase-1, GSDMD, GSDMD-N, pro-IL-18, mature IL-18, pro-IL-1β, and mature IL-1β was significantly upregulated in the MI mouse hearts as well (Fig. 2(c)). An immunohistochemical analysis of the mouse hearts revealed that the expression of NLRP3 and caspase-1 were also markedly upregulated in the MI group (Fig. 2(d)). In addition, similar changes on IL-18 and IL-1β were consistently observed in the MI mouse serum (Fig. 2(e)), showing the induction of cardiomyocyte pyroptosis.

LPS was used to induce an inflammatory response in the cardiomyocytes in order to mimic myocardial inflammation after MI. A TUNEL staining analysis of the cardiomyocytes further confirmed that the LPS had induced nuclear chromosomal DNA breakage (Fig. S1(a) in Appendix A). The electron microscopy images showed karyopyknosis, mitochondrial swelling, and membranolysis

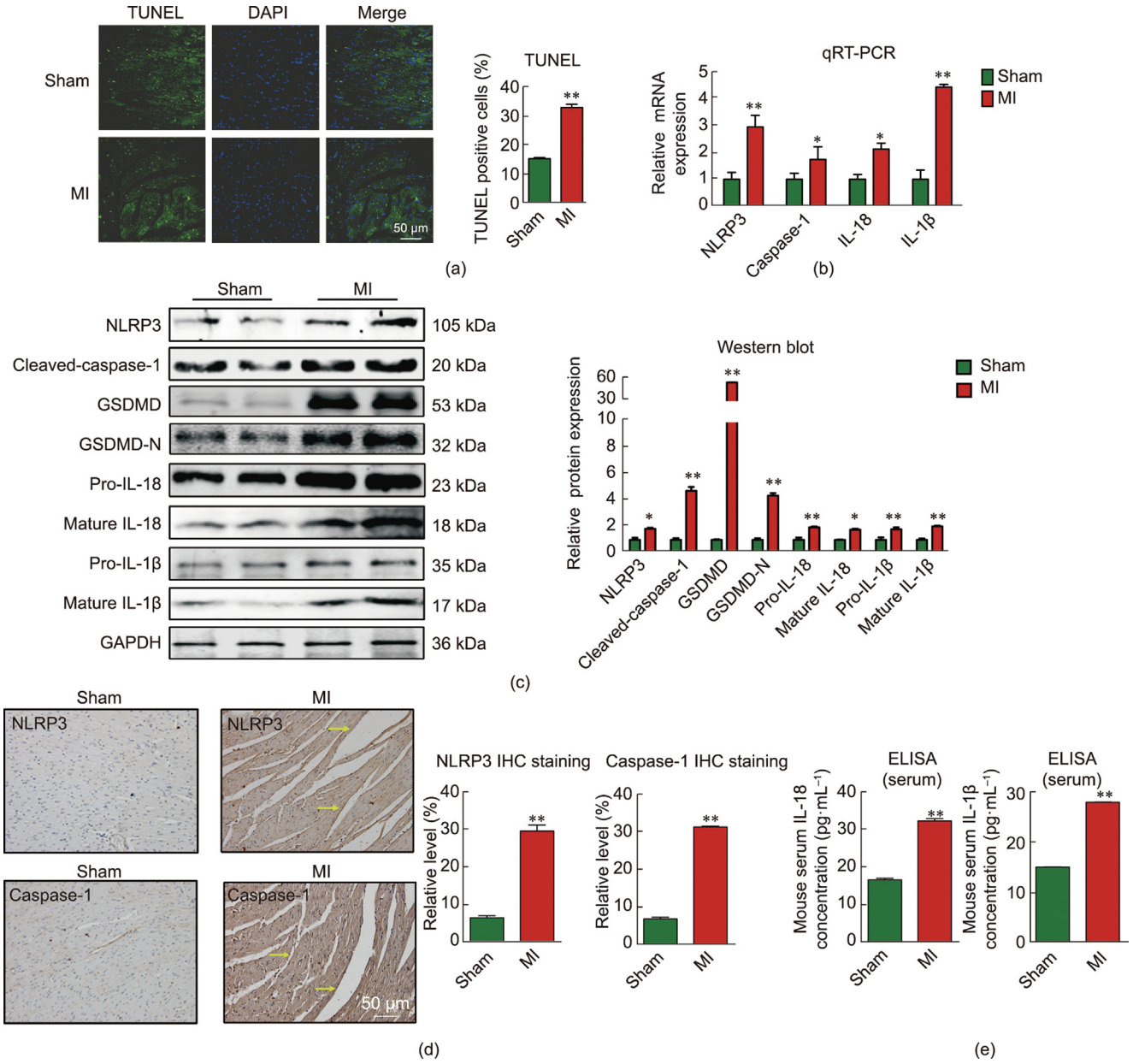

Fig. 2. Cardiomyocyte pyroptosis occurs in MI hearts. (a) Representative images were stained by TUNEL, showing cells with nuclear chromosomal DNA fragmentation in the sham and MI groups (green: TUNEL-positive cells; blue: DAPI; n = 3). (b) Relative mRNA levels in the sham and MI hearts (n = 4 to n = 8; $^{*}P$ < 0.05, $^{**}P$ < 0.01, compared with sham, mean ± SEM). (c) Relative protein levels of NLRP3, cleaved caspase-1, GSDMD, GSDMD-N, pro-IL-18, mature IL-18, pro-IL-1β, mature IL-1β, and GAPDH in the sham and MI groups ($^{*}P$ < 0.05, $^{**}P$ < 0.01, compared with sham; n = 3 to n = 9; mean ± SEM). (d) NLRP3 and caspase-1 levels as shown by immunohistochemical staining in sham and MI hearts (yellow arrow indicates positive cells; $^{**}P$ < 0.01, compared with sham; mean ± SEM; n = 3). (e) Concentration of IL-18 and IL-1β in sham and MI mouse serum detected by ELISA assay ($^{**}P$ < 0.01, compared with sham; n = 4 to n = 6; mean ± SEM).

in the LPS-treated cardiomyocytes (Fig. S1(b) in Appendix A). A qRT-PCR analysis of the cardiomyocytes revealed that the expression of caspase-1 was markedly augmented at the mRNA level in the LPS-treated group, and similar changes in NLRP3, IL-18, and IL-1β were consistently demonstrated (Fig. S1(c) in Appendix A). Meanwhile, the expression of NLRP3, cleaved caspase-1, GSDMD, GSDMD-N, pro-IL-18, mature IL-18, pro-IL-1β, and mature IL-1β protein levels was significantly increased in the LPS-treated cardiomyocytes (Fig. S1(d) in Appendix A). An immunofluorescence assay showed that the expression of NLRP3 and caspase-1 was markedly increased in the LPS-treated cardiomyocytes (Fig. S1(e) in Appendix A).

3.3. Effect of CPAL deficiency on cardiac protection

We then further explored the key role of lncRNAs in the inflammatory process after MI. We began by measuring the levels of differential expression of lncRNAs that may be associated with CVDs [10], including AK009126 (CPAL), AK157022, AK086435, AK156356, AK076765, AK035575, AK044386, AK141702, AK0158845, ENSMUST00000148132, ENSMUST00000101162, ENSMUST00000137198, and ENSMUST00000143898 in both the sham and MI hearts or inflammatory conditions. The results revealed that CPAL exhibited the most pronounced deregulation in the MI hearts and inflammatory process (Figs. 3(a) and (b)). FISH assays indicated that CPAL was distributed in both the nucleus and cytoplasm of the cardiomyocytes and was increased after LPS treatment in neonatal cardiomyocytes (Fig. 3(c)). Based on the above findings, we further explored whether the alteration of CPAL is related to cardiomyocyte metabolic alterations and pyroptosis by means of the experimental procedure shown in Fig. 3(d). In an *in vivo* study, AAV9-sh-NC and AAV9-sh-CPAL were delivered into the mouse via tail vein injection; then, four weeks after AAV9-sh-CPAL infection (1×10^{12} vg·mL^{-1}, 100 μL), the expression efficiency of CPAL was verified by qRT-PCR in various tissues. The results showed that CPAL was successfully knocked down in the myocardium (Fig. S2 in Appendix A). Subsequently, we constructed an MI mouse model by means of LAD coronary artery ligation for 24 h. 2,3,5-TTC staining showed that knocking down CPAL reduced the infarct size in MI-injured mouse hearts (Fig. 3(e)). Echocardiograph measurements revealed that the EF and FS were markedly declined in MI mice at 24 h but were conspicuously increased in the AAV9-sh-CPAL administration group, indicating the cardiac protection of CPAL deletion (Fig. 3(f)). Mice in the sham groups did not show histological lesions in the heart. All mice in the MI group showed mild inflammatory foci in the heart, and these alterations were significantly alleviated in the CPAL knockdown group (Fig. 3(g)). Moreover, to measure the function of CPAL on the ultrastructure of the cardiomyocytes, electron microscopy was performed. We found that swollen mitochondria and karyopyknosis appeared in the MI hearts. CPAL deletion significantly alleviated these changes, suggesting that CPAL deletion reduced the development of inflammation and protected the heart against ischemic injury after MI surgery (Fig. 3(h)).

3.4. Effect of CPAL deficiency on cardiomyocyte metabolism

Ventricular remodeling after MI is a chronic and complex process in which the energy metabolism is regulated by many factors. Here we first explored whether CPAL is involved in the NFκB-related myocardial energy metabolic process. We found that the ATP level was reduced in the border zone of infarcted hearts when examined by means of ELISA; however, these harmful changes were attenuated visibly by the deletion of CPAL (Fig. 4(a)). In addition, an abnormal glucose and lipid metabolism exists in myocardial ischemia. The evidence revealed that the expression of *HK1* and *CD36* at the mRNA level was visibly downregulated in the MI group, which was prevented by CPAL deletion (Figs. 4(b) and (c)). Meanwhile, GLUT4, HK1, and CD36 were significantly downregulated in the MI hearts at the protein level, which was prevented by CPAL deletion, as depicted in Figs. 4(d)–(f). Taken together, these data suggest that CPAL deficiency is beneficial for protecting the glucose and lipid metabolism and replenishing the ischemic myocardium, and thereby contributes to the reduction of myocardial ischemic injury.

3.5. CPAL deletion reduces cardiomyocyte pyroptosis in MI mice

To ascertain whether CPAL deletion exerts a protective effect on cardiomyocyte pyroptosis in MI hearts, TUNEL staining was performed and revealed myocardial ischemia-caused cell death, where CPAL deletion attenuated the cell death (Fig. 5(a)). As shown in Fig. 5(b), CPAL deletion decreased the mRNA expression of NLRP3, caspase-1, IL-18, and IL-1β, compared with those in the MI hearts. Consistently, CPAL deletion reduced the protein levels of NLRP3, cleaved caspase-1, GSDMD, GSDMD-N, pro-IL-18, mature IL-18, pro-IL-1β, and mature IL-1β, compared with those of MI mice, as shown by Western blot analysis (Fig. 5(c)). Serum samples were collected from each group for measuring the IL-18 and IL-1β levels using ELISA; the results revealed that the serum levels of IL-18 and IL-1β were visibly decreased in CPAL knocked-down MI mice, relative to the MI samples (Fig. 5(d)). Consistently, immunohistochemical analysis revealed a significant decrease in NLRP3 and caspase-1 protein level, respectively, in CPAL deletion mice compared with that of MI mice (Fig. 5(e)).

3.6. CPAL silencing reduced pyroptosis in vitro

In cardiomyocytes, knockdown of CPAL was performed using si-CPAL (Fig. S3 in Appendix A). A severe loss of cardiomyocytes was observed in the LPS group. However, si-CPAL treatment significantly improved cardiomyocyte survival, as revealed by TUNEL staining (Fig. 6(a)). As shown in Fig. 6(b), the cells exhibited varying degrees of ultrastructural changes, including karyopyknosis, mitochondrial swollen degeneration, and damage to the membrane after LPS stimulation, and these alterations were reversed by si-CPAL. Furthermore, Western blot results showed that CPAL silencing attenuated the expression of NLRP3, cleaved caspase-1, GSDMD, GSDMD-N, pro-IL-18, mature IL-18, pro-IL-1β, and mature IL-1β at the protein level compared with the LPS group (Fig. 6(c)). Consistently, the immunofluorescence assay showed decreases in NLRP3 and caspase-1 protein levels in si-CPAL-treated neonatal mouse cardiomyocytes compared with those that were si-NC-treated alone (Fig. 6(d)). In addition, we analyzed the effect of CPAL on the release of LDH and found that CPAL silence inhibited the level of LDH release that had increased due to LPS. These results indicated that an increase in the plasma membrane permeability is involved in CPAL-mediated cardiomyocyte pyroptosis (Fig. 6(e)).

3.7. CPAL as an upstream activator of NFκB

In order to explore the key mechanism of CPAL in regulating cardiomyocyte pyroptosis, we performed a theoretical analysis for RNA–protein binding using the catRAPID database. The analysis revealed a high probability of a CPAL and NFκB interaction at 76–127 and 209–260 nt (Fig. 7(a)). This initial analysis led us to examine the functional relationship between CPAL and NFκB. We then performed RIP to determine whether CPAL could directly bind to NFκB. The results clearly showed the existence of such an interaction—namely, the immunoprecipitation of NFκB in combination with an appreciable amount of CPAL (Fig. 7(b)), which indicated that CPAL has a strong and specific affinity for NFκB. After this,

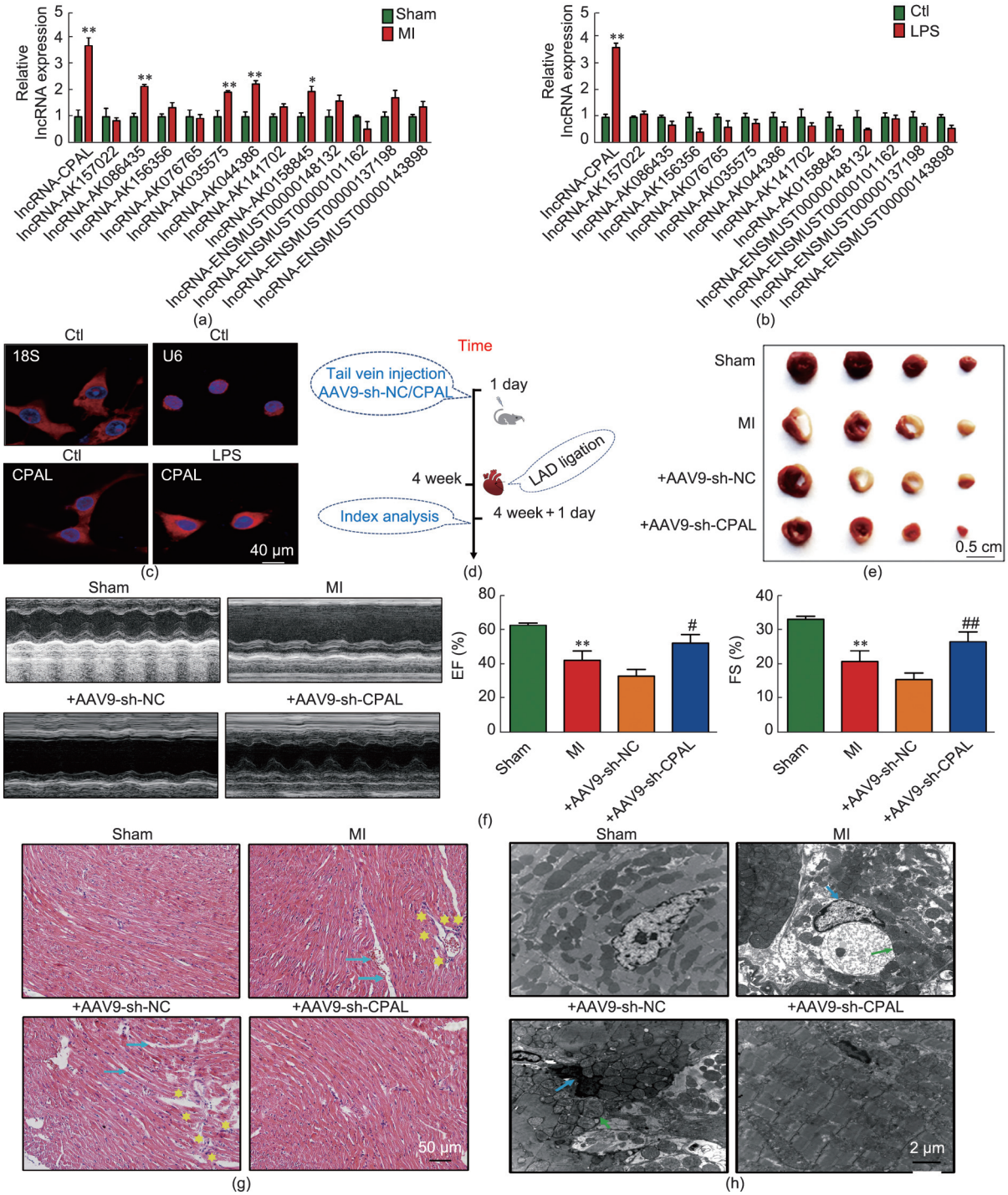

Fig. 3. CPAL is upregulated in MI hearts and under inflammatory conditions. (a) lncRNAs expression analysis of the sham mouse hearts relative to MI by qRT-PCR assay (n = 3 to n = 6; $^{*}P$ < 0.05, $^{**}P$ < 0.01, compared with sham). (b) Verification of the lncRNAs expression analysis in cardiomyocytes after treatment with LPS (50 nmol·L^{-1}) for 12 h or untreated (n = 3 to n = 6; $^{**}P$ < 0.01, compared with control (Ctl) group). (c) FISH staining of the CPAL-specific probe in cardiomyocytes (18S is a cytoplasmic marker, and U6 is a nuclear marker n = 3 to n = 5). (d) Schematic diagram of the experimental procedure of the *in vivo* study. (e) Recombinant adeno-associated virus (serotype 9; AAV9) vector carrying the shRNA (AAV9-sh-CPAL) to knock down endogenous CPAL in MI mice. TTC staining of infarction border zones of mouse hearts in the sham, MI, +AAV9-sh-NC, and +AAV9-sh-CPAL groups. (f) Echocardiogram, EF, and FS analysis of sham, MI, +AAV9-sh-NC, and +AAV9-sh-CPAL mice ($^{**}P$ < 0.01, compared with sham group; $^{\#}P$ < 0.05, $^{\#\#}P$ < 0.01, compared with +AAV9-sh-NC group; n = 5 to n = 8; mean ± SEM). (g) H&E staining of cross-sectional slices derived from the sham, MI, +AAV9-sh-NC, and +AAV9-sh-CPAL hearts (blue arrow indicates a larger intercellular space, and yellow stars indicate inflammatory cell infiltration; n = 3 to n = 4). (h) TEM micrograph showing the ultrastructural changes in the myocardium in each group mice (blue arrow: karyopyknosis; green arrow: mitochondrial swelling; n = 4).

we examined whether CPAL performs any direct action in NFκB activities in addition to protein interactions. We found that the expression of P-NFκB was visibly downregulated after CPAL depletion at the protein level, while the protein expression of the total NFκB was not significantly changed. (Fig. 7(c)). Similar downregulation of P-NFκB was also observed in CPAL knockdown MI mice by means of immunohistochemical analysis (Fig. 7(d)). *In vitro*, CPAL siRNA was performed to verify the regulatory function of CPAL

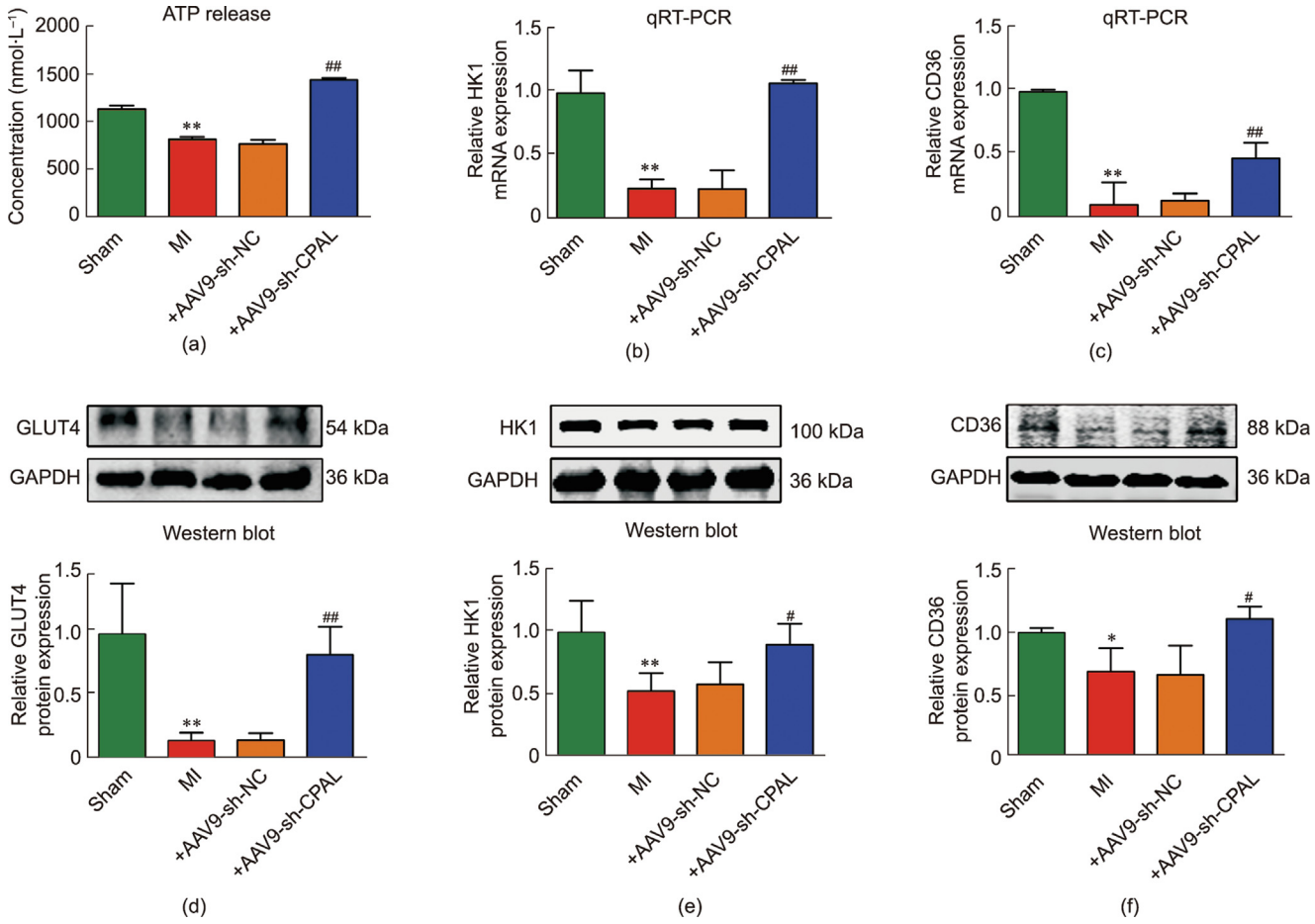

Fig. 4. CPAL regulates the myocardium metabolism after myocardial infarction in mice. (a) ATP levels in the homogenate of heart tissue from the sham, MI, +AAV9-sh-NC, and +AAV9-sh-CPAL groups (n = 5; $^{**}P < 0.01$; $^{\#\#}P < 0.01$, compared with +AAV9-sh-NC group). (b, c) Expression of *HK1* and *CD36* at the mRNA levels in the infarct border zones of the left ventricular from each group at 24 h after MI operation ($^{**}P < 0.01$, compared with sham group; $^{\#\#}P < 0.01$, compared with +AAV9-sh-NC group; n = 3 to n = 5: mean ± SEM). (d–f) Relative protein levels of GLUT4, HK1, and CD36 in each group. Protein expressions were normalized to GAPDH ($^{*}P < 0.05$, $^{**}P < 0.01$, compared with sham group; $^{\#}P < 0.05$, $^{\#\#}P < 0.01$, compared with +AAV9-sh-NC group; n = 3; mean ± SEM).

on NFκB. The result indicated that the expression of P-NFκB at the protein level was visibly downregulated after si-CPAL treatment under LPS condition compared with +si-NC group (Fig. 7(e)); however, the expression of total NFκB was not changed. Similar results were shown in P-NFκB P65 by means of immunofluorescence analysis (Fig. 7(f)). Immunofluorescence staining showed that treatment with LPS led to the accumulation of P-NFκB P65 in the nuclei of cardiomyocytes, while CPAL silencing inhibited this phenomenon. These findings suggest that CPAL may activate the NFκB function by promoting the phosphorylation of NFκB, thereby allowing NFκB to enter the nucleus. In order to confirm that NFκB phosphorylation is directly induced by CPAL binding to site1, CTCGGAGAGACCCTGGAGGGACCAGGACCACTCTTGTCTCGCCTGGACCTGC, and site2, TGTCTGAAGAAAAATGCTGGCCACTAATCGTTTGCCTCGAAGGAGTCTGAGG, oligodeoxynucleotide (ODN) technology was adopted. Two sequence segments of CPAL-ODNs were constructed to specifically target and mask the binding sites of NFκB, labeled CPAL-ODN-1 (masking site1) and CPAL-ODN-2 (masking site2). The two ODNs were designed to be fully complementary to the two predicted CPAL binding sites respectively. Co-transfection with CPAL and the ODNs failed to affect the P-NFκB level (Fig. 7(g)). This result indicates that CPAL can physically bind with NFκB and can induce the phosphorylation of NFκB by binding the sites (site1: 76–127 nt and site2: 209–260 nt).

3.8. Suppression of NFκB reduced LPS-led neonatal mouse cardiomyocyte pyroptosis

In order to explore the role of NFκB in LPS-mediated neonatal mouse cardiomyocyte pyroptosis, we further explored whether cardiomyocyte pyroptosis was reversed by SN50, a cell-permeable inhibitor of NFκB translocation, and Ac-YVAD-CMK, a potent caspase-1 inhibitor (Fig. 8(a)). We found that SN50 significantly inhibited pro-caspase-1 and cleaved caspase-1 expression at the protein level in LPS-treated neonatal mouse myocardial cells. This finding means that NFκB inhibition significantly inhibits caspase-1 protein expression, suggesting that caspase-1 may be the downstream gene of NFκB transcription regulation. Ac-YVAD-CMK visibly suppressed the expression of NLRP3, pro-caspase-1, cleaved caspase-1, GSDMD, GSDMD-N, pro-IL-18, mature IL-18, pro-IL-1β, and mature IL-1β in cardiomyocytes, indicating that the inhibitor of caspase-1 in cardiomyocytes significantly inhibited the expression of genes related to pyroptosis. The expression levels of NLRP3, pro-caspase-1, cleaved caspase-1, GSDMD, GSDMD-N, pro-IL-18, mature IL-18, pro-IL-1β, and mature IL-1β in the cardiomyocytes were visibly lower when the two inhibitors worked together, indicating that NFκB is involved in inflammatory responses and pyroptosis by regulating the expression of caspase-1 in myocardial cells. Finally, we

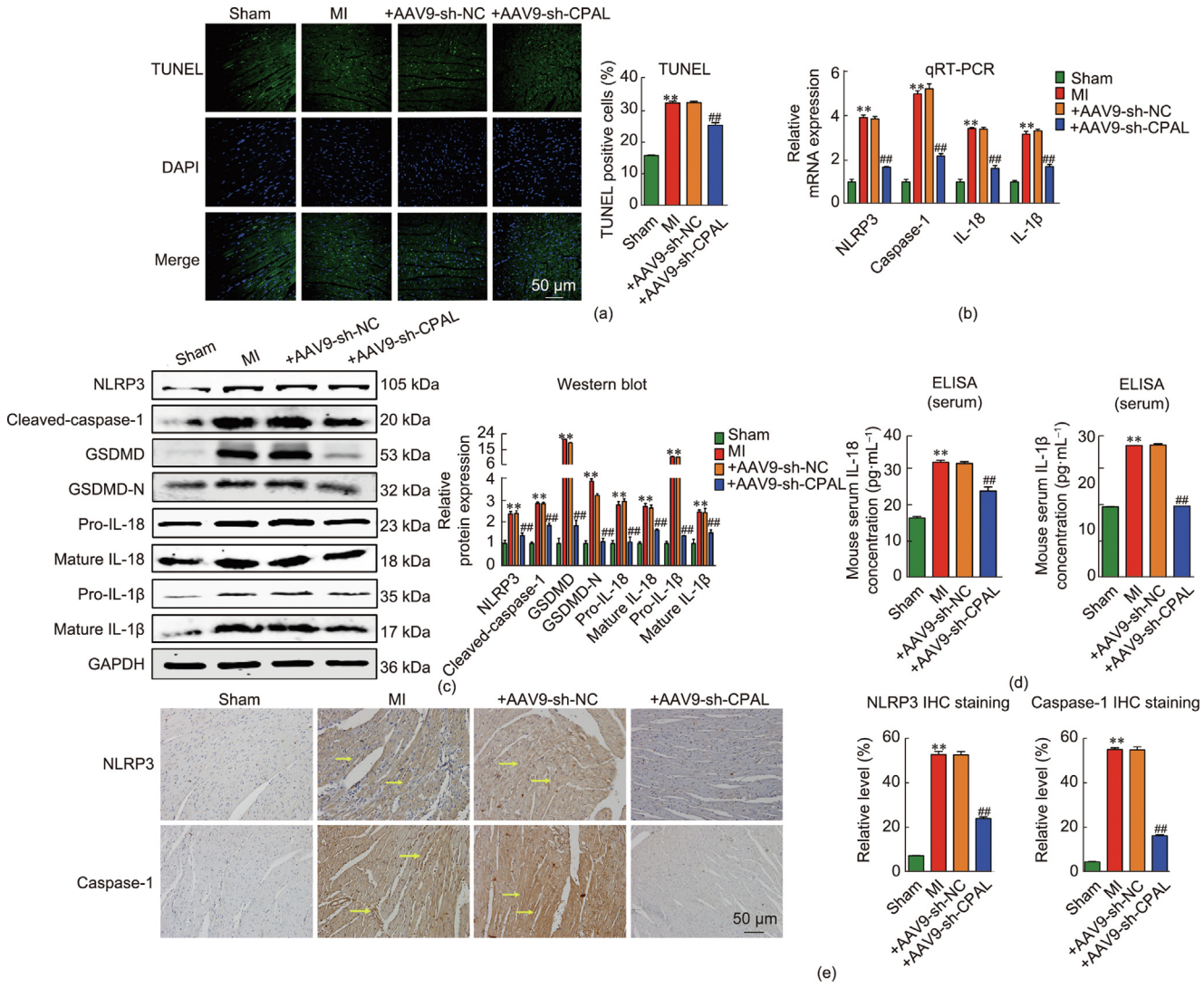

Fig. 5. Downregulation of CPAL-inhibited pyroptosis. (a) Representative TUNEL images showing cells with chromosomal DNA fragmentation in each group (green: TUNEL-positive cells; blue: DAPI; n = 3 to n = 4 $^{**}P$ < 0.01, compared with sham group; $^{\#\#}P$ < 0.01, compared with +AAV9-sh-NC group; mean ± SEM). (b) NLRP3, *Caspase-1*, *IL-18*, and *IL-1β* at the mRNA levels in the infarct border zones of the left ventricular from each group at 24 h after MI operation ($^{**}P$ < 0.01, compared with sham group; $^{\#\#}P$ < 0.01, compared with +AAV9-sh-NC group; mean ± SEM; n = 6 to n = 10 mice for each group). (c) Relative protein levels of NLRP3, cleaved caspase-1, GSDMD, GSDMD-N, pro-IL-18, mature IL-18, pro-IL-1β, and mature IL-1β in mouse hearts. Protein expressions were normalized to GAPDH ($^{**}P$ < 0.01, compared with sham group; $^{\#\#}P$ < 0.01, compared with +AAV9-sh-NC group; n = 3 to n = 6; mean ± SEM). (d) Concentration of IL-18 and IL-1β in each mouse serum ($^{**}P$ < 0.01, compared with sham; $^{\#\#}P$ < 0.01, compared with +AAV9-sh-NC group; mean ± SEM; n = 4 to n = 6 mice for each group). (e) Immunohistochemical staining of NLRP3 and caspase-1 protein in the infarct border zones of the left ventricular ($^{**}P$ < 0.01, compared with sham group; $^{\#\#}P$ < 0.01, compared with +AAV9-sh-NC group; n = 3 to n = 4; mean ± SEM).

investigated whether NFκB has any direct effects on *Caspase-1* activities, apart from regulating expression and the mechanism of this caspase-1-mediated regulation of expression. Therefore, we used the TF-Protein Interaction Prediction (PROMO) database to perform a theoretical analysis of DNA–protein binding. The analysis using the PROMO tools revealed that the proximal regions of the *Caspase-1* DNA promoter harbor putative NFκB binding sequences near site1 and site2. These sequences are conserved among humans, rats, and mice. ChIP assays displayed the recruitment of NFκB to the proximal promoter regions of *Caspase-1* at site1 and site2, suggesting that NFκB has a strong affinity for *Caspase-1* (Fig. 8(b)). In order to confirm that the caspase-1 increase was directly induced by NFκB binding to both site1 and site2, ODN technology was adopted. Two sequence segments of caspase1-ODNs were designed, respectively based on the two predicted caspase-1 binding sites, and were constructed to specifically target and mask the binding sites of NFκB, labeled caspase1-ODN-1 (masking site1) and caspase1-ODN-2 (masking site2). After co-transfection with ODNs-caspase1 in LPS-treated neonatal mouse cardiomyocytes, LPS treatment failed to affect the expression levels of pro-caspase-1, cleaved caspase-1, and GSDMD-N (Fig. 8(c)). This result indicates that NFκB can directly bind with *Caspase-1* and can induce *Caspase-1* transcription by binding the sites (site1: −846–836 bp and site2: −1544–1555 bp).

4. Discussion

For the first time, we have uncovered the critical pathophysiological relevance of the lncRNA CPAL and its precise mechanisms in the setting of MI. This study demonstrated that CPAL was upregulated in MI hearts and induced visible negative impacts on heart remodeling and disfunction. Knockdown of endogenous CPAL partially rescued the glucose and lipid metabolism alterations of the ischemic myocardium, and inhibited the MI-induced cardiomyocyte pyroptosis. Furthermore, we found that CPAL directly interacted with NFκB protein and increased its

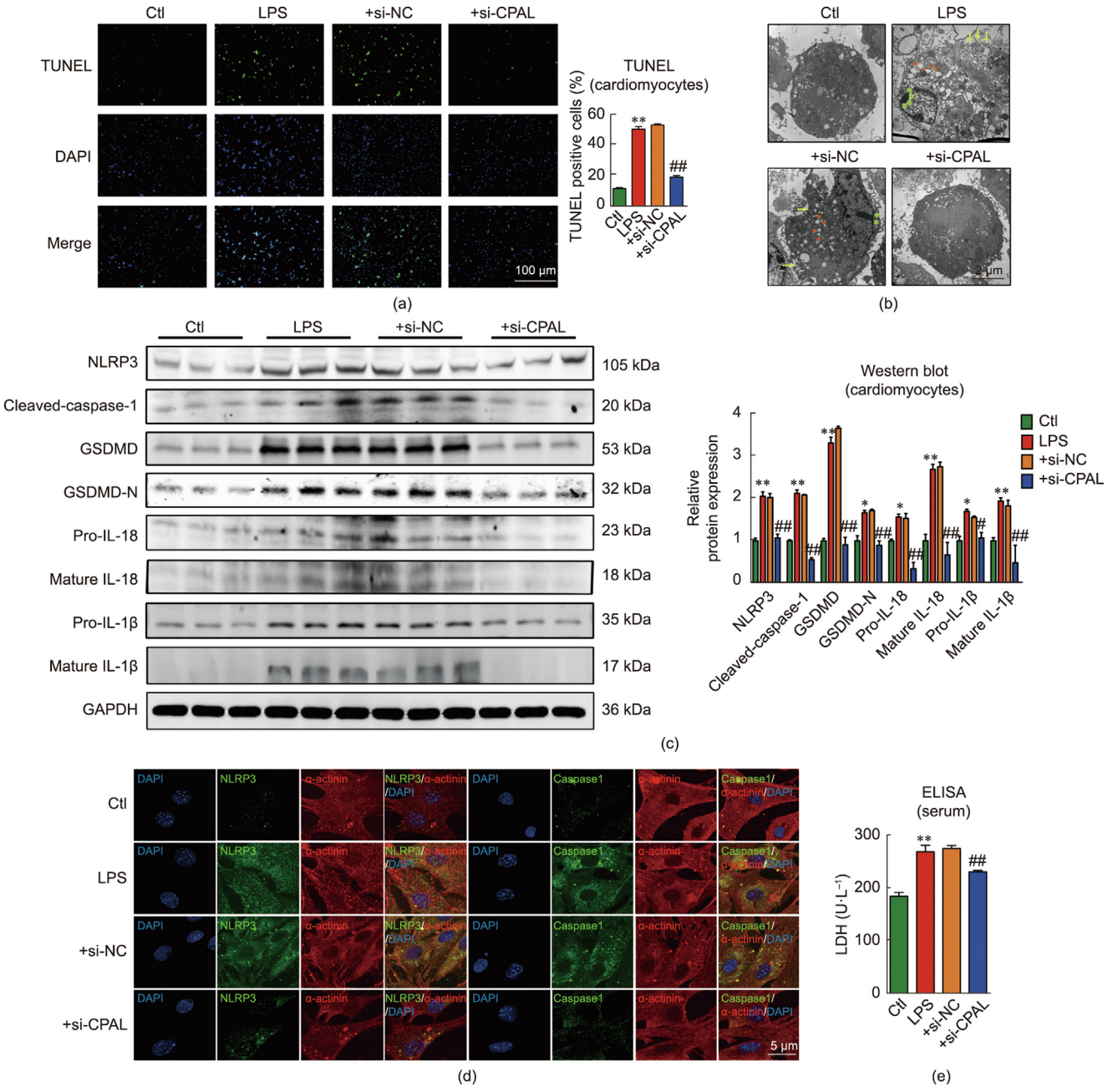

Fig. 6. CPAL silencing reduced LPS-induced cardiomyocyte pyroptosis. (a) Representative images stained by TUNEL and percentage analysis of TUNEL-positive cardiomyocytes in the control, LPS, +si-NC, and +si-CPAL groups (green: TUNEL-positive cells; blue: DAPI $^{**}P < 0.01$, compared with control group; $^{\#\#}P < 0.01$, compared with +si-NC group; $n = 3$ to $n = 6$; mean ± SEM). (b) TEM micrograph showing the ultrastructural changes in neonatal mouse cardiomyocytes in the control, LPS, +si-NC, and +si-CPAL groups (green stars: karyopyknosis, red triangles: mitochondrial vacuole, yellow arrow: membranolysis $n = 3$). (c) Western blot analysis of NLRP3, cleaved caspase-1, GSDMD, GSDMD-N, pro-IL-18, mature IL-18, pro-IL-1β, and mature IL-1β in the control, LPS, +si-NC, and +si-CPAL groups ($n = 3$ to $n = 6$, $^{*}P < 0.05$, $^{**}P < 0.01$, compared with control group; $^{\#}P < 0.05$, $^{\#\#}P < 0.01$ compared with +si-NC group; mean ± SEM). (d) Immunofluorescence staining for NLRP3/caspase-1-α-actinin in the neonatal mouse cardiomyocytes of control, LPS, +si-NC, and +si-CPAL groups (green: NLRP3/caspase-1, red: α-actinin, blue: DAPI $n = 4$). (e) Concentration of LDH release in each group of cell medium ($n = 4$; $^{**}P < 0.01$, compared with control group; $^{\#\#}P < 0.01$, compared with +si-NC group; mean ± SEM).

phosphorylation. Then, the phosphorylated NFκB was transported from the cytoplasm into the nucleus and promoted its transcription activity, which might underlie the regulation of cardiac metabolism alteration and pyroptosis by CPAL in MI.

In the process of MI, cardiomyocytes subjected to ischemia stimuli undergo energy metabolism disorders, oxidant stress, cell deaths, inflammation, and so forth. The glucose and lipid metabolism disorders play a vital role in the development of cardiac remodeling in diabetes and others [31]. Changes in the glucose and lipid metabolism in the heart have been shown to trigger cardiomyocyte apoptosis, myocardial hypertrophy, and heart fibrosis [31]. In addition, inflammation is involved in the repairing and remodeling of infarcted hearts [32]. The sequential activity patterns of an inflammatory reaction release inflammatory cytokines and alter metabolic disorders, which accelerate myocardial remodeling in the setting of MI [33]. In this study, we found that cardiomyocytes from the border zone of MI hearts exhibited reduced ATP production, altered expression of CD36, HK1, and

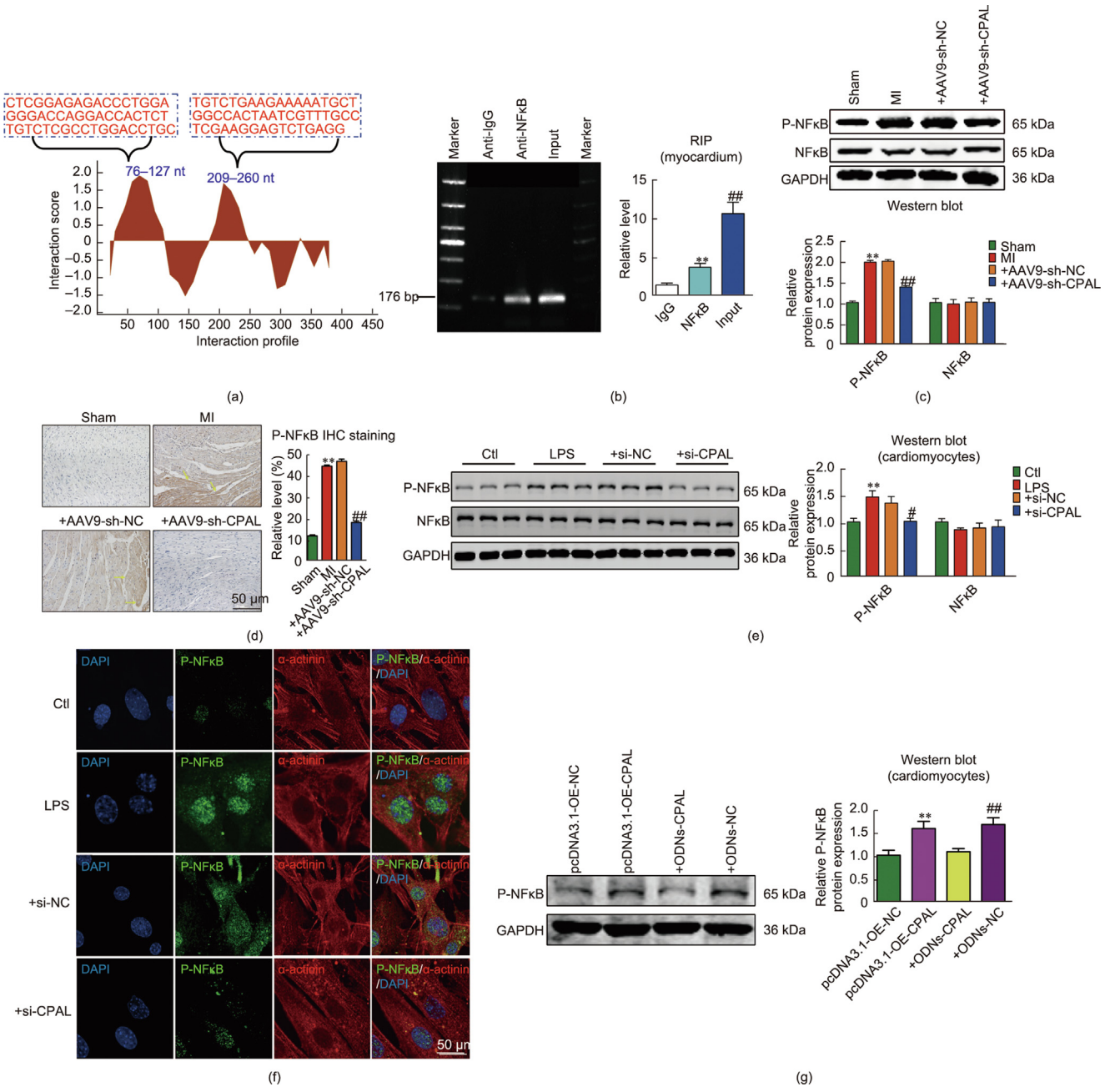

Fig. 7. CPAL is an upstream regulator of NFκB. (a) Two specific regions (76–127 nt and 209–260 nt) of CPAL that were found to bind with NFκB using the online prediction website. (b) RIP analysis for CPAL-NFκB interaction. Immunoprecipitation of NFκB acquired a large amount of CPAL ($^{**}P$ < 0.01, compared with anti-IgG; n = 3). (c) Expression of P-NFκB and NFκB at the protein levels in each group ($^{**}P$ < 0.01, compared with sham group; $^{\#\#}P$ < 0.01, compared with +AAV9-sh-NC group; n = 4 to n = 6). (d) Immunohistochemical staining of P-NFκB protein in the infarct border zones of the left ventricular ($^{**}P$ < 0.01, compared with sham group; $^{\#\#}P$ < 0.01, compared with +AAV9-sh-NC group; n = 3 to n = 4). (e) Expression of P-NFκB and NFκB at the protein level in cardiomyocytes of control, LPS, +si-NC, and +si-CPAL groups ($^{**}P$ < 0.01, compared with control; $^{\#}P$ < 0.05, compared with LPS group; n = 9). (f) Staining for P-NFκB (green) and α-actinin (red) proteins in the cardiomyocytes of control, LPS, +si-NC, and +si-CPAL groups (blue: DAPI; n = 4). (g) P-NFκB expression in the neonatal mouse cardiomyocytes of pcDNA3.1-OE-NC, pcDNA3.1-OE-CPAL, +ODNs-CPAL, and +ODNs-NC groups ($^{**}P$ < 0.01, compared with pcDNA3.1-OE-NC; $^{\#\#}P$ < 0.01, compared with pcDNA3.1-OE-CPAL; n = 5).

GLUT4, and cardiomyocyte inflammatory injury. These data indicated that glucose and lipid metabolism disorders and cardiomyocyte pyroptosis were present in the ischemic myocardium of MI mice.

Recent studies have suggested that lncRNAs are important regulators of metabolic responses and physiological homeostasis in various organs [34]. However, the regulatory lncRNAs involved in the cardiac energy metabolism and inflammation of MI hearts had not been explored. In this study, CPAL, a new member of MI-associated lncRNAs that is conserved among human, rats, and mouse, was identified as being considerably increased in mice with MI. The results revealed the key pathophysiological roles of CPAL in the regulation of glucose and lipid metabolism disorders and inflammatory processes in the cardiac remodeling of MI. More specifically, the silencing of CPAL in MI attenuated glucose and lipid metabolism disorder and cardiomyocyte pyroptosis in the

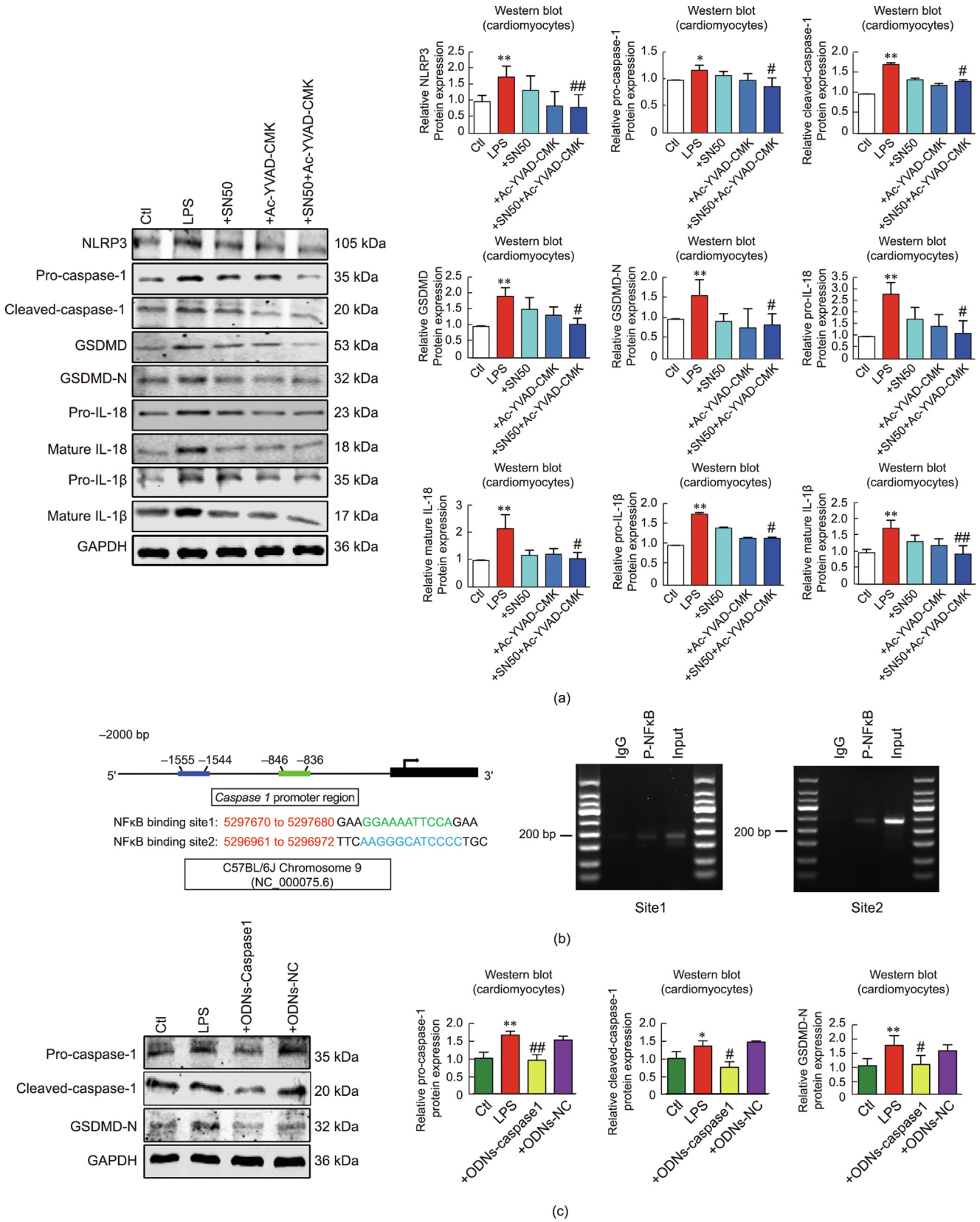

Fig. 8. Inhibition of NFκB alleviated LPS-induced cardiomyocyte pyroptosis. (a) Expression of NLRP3, pro-caspase-1, cleaved caspase-1, GSDMD, GSDMD-N, pro-IL-18, mature IL-18, pro-IL-1β, and mature IL-1β at the protein level after treatment with SN50 (5 μg·mL^{-1}, 24 h) and Ac-YVAD-CMK (50 μg·mL^{-1}, 24 h) under LPS conditions ($^{*}P$ < 0.05, $^{**}P$ < 0.01, compared with control, $^{\#}P$ < 0.05, $^{\#\#}P$ < 0.01, compared with LPS group, n = 3 to n = 5, mean ± SEM). (b) NFκB positively activates caspase-1 by binding to the *caspase*-1 promoter. (left) Conserved NFκB DNA binding sites in the *caspase*-1 promoters. PROMO tools indicating potential binding sites at 2000 bp upstream in the proximal region of *caspase*-1 promoters. (right) Results of ChIP assays indicate the recruitment of NFκB to the proximal promoter regions of *caspase* site1 and site2 (n = 4). (c) Cleaved caspase-1, pro-caspase-1, and GSDMD-N protein expression in the neonatal mouse cardiomyocytes of control, LPS, +ODNs-caspase1, and +ODNs-NC groups ($^{*}P$ < 0.05, $^{**}P$ < 0.01 compared with control; $^{\#}P$ < 0.01, $^{\#\#}P$ < 0.01 compared with LPS, n = 3 to n = 4).

post-infarcted hearts of mice, which suggests CPAL as a new therapy target for the prevention of cardiac injury in MI.

NFκB is a crucial transcription factor in vascular endothelial cells and myocardial cells [35]. It binds with IκB (an inhibitory protein), which exists in the form of a homodimer under normal physiological conditions and is inactive [36,37]. In the activation process of pyroptosis, Nod-like receptors (NLRs), pyrin, and AIM2 bind to the ASC domain and activate pro-caspase-1 to generate active caspase-1 [38]. lncRNAs usually interact with mRNAs by sharing the same transcription factor [8]. It has been reported that the lncRNA MALAT1 downregulates the NFκB signaling pathway by acting as a ceRNA, and that its expression is decreased with aging [39]. In the present study, we find that lncRNA CPAL binds with NFκB and breaks the bond between NFκB and IκB, activates NF-κB through phosphorylation at Ser536, and causes the P-NF-κB to transfer from the cytoplasm to the nucleus, where it binds with the specific pro-caspase-1 sites and regulates transcriptional activity. In addition, previous research has shown that NLRP3 is a family member of the NLRs in intracellular proteins, which plays an important role in activating caspase-1-containing complexes—the so-called inflammasomes [39,40]. Furthermore, NFκB activation is dependent on TLR-induced NLRP3 expression [41]. Our findings showed that CPAL deletion attenuated the phosphorylation of NFκB, and inhibited the expression of NLRP3. However, future research is needed to further confirm this point, and we will continue to investigate the relationship between CPAL and NFκB phosphorylation.

In addition, NFκB is a key regulator of myocardial glucose and lipid metabolism. The downstream target genes of NFκB are also involved in glycolipids and energy metabolism. Zhu et al. [16] reported that the inhibition of NFκB activation by QNZ improved the glucose uptake through GLUT4 activation and inhibited chondrocyte degeneration. Wu et al. [42] found that LPS enhanced glycolysis and promoted metastasis through the NFκB/Snail/HK3 signaling pathway in colorectal cancer cells. Han et al. [43] suggested that a high level of CD36 promoted an inflammatory reaction through NFκB mediated by lipid accumulation and metabolism reprogramming. In our study, CPAL deletion enhanced glucose and fatty acid utilization and improved the energy metabolism by regulating GLUT4/HK1 and CD36 protein expression in ischemic myocardium. To sum up, this study revealed that CPAL, as a detrimental lncRNA, promoted glucose and lipid metabolism disorders and cardiomyocyte pyroptosis in the process of MI by targeting the P-NFκB p65 signaling pathway. The sequence of CPAL-mediated metabolic alterations and cardiomyocyte pyroptosis via NFκB is not very clear at present, so it remains to be further discussed in the following study.

5. Conclusions

The findings of this study indicate that CPAL can be not only a biomarker or predictor of MI but also a key regulator of cardiomyocyte pyroptosis and of glucose and lipid metabolism after MI and, perhaps, in other CVDs. This study set out to assess the protective effect of CPAL deficiency on cardiac function and to open up an exciting opportunity for improving the heart dysfunction induced by ischemia/inflammation. The results imply that CPAL could be a crucial therapeutic target for improving cardiac function in the setting of MI.

Acknowledgments

This work was supported by the Heilongjiang Touyan Innovation Team Program (Ning Wang, Benzhi Cai, and Baofeng Yang), by Harbin Medical University Marshal Initiative Funding (HMUMIF-21026 to Ning Wang), and by the Foundation of Heilongjiang postdoctoral (LBH-Z18166 to Jiamin Li).

Compliance with ethics guidelines

Jiamin Li, Hongru Xue, Ning Xu, Liling Gong, Ming Li, Sijia Li, Di Huang, Qingwei Zhang, Pengyu Li, Qingsui Li, Hang Yu, Yining Liu, Yadong Xue, Haixin Chen, Jiali Liu, Wanyu Zhang, Mingbin Liu, Siyu Chang, Xianzhi Lang, Xingmiao Zhao, Weijie Du, Benzhi Cai, Ning Wang, and Baofeng Yang declare that they have no conflict of interest or financial conflicts to disclose.

Appendix A. Supplementary data

Supplementary data to this article can be found online at https://doi.org/10.1016/j.eng.2022.08.012.

References

[1] Alakoski T, Ulvila J, Yrjölä R, Vainio L, Magga J, Szabo Z, et al. Inhibition of cardiomyocyte Sprouty1 protects from cardiac ischemia-reperfusion injury. Basic Res Cardiol 2019;114(2):7.
[2] Pinaire J, Azé J, Bringay S, Cayla G, Landais P. Hospital burden of coronary artery disease: trends of myocardial infarction and/or percutaneous coronary interventions in France 2009–2014. PLoS One 2019;14(5):e0215649.
[3] Virani SS, Alonso A, Aparicio HJ, Benjamin EJ, Bittencourt MS, Callaway CW, et al.; AHA Council on Epidemiology and Prevention Statistics Committee and Stroke Statistics Subcommittee. Heart disease and stroke statistics—2021 update: a report from the American Heart Association. Circulation 2021;143(8):e254–743.
[4] Cai B, Ma W, Ding F, Zhang L, Huang Q, Wang X, et al. The long noncoding RNA CAREL controls cardiac regeneration. J Am Coll Cardiol 2018;72(5):534–50.
[5] Zhang Y, Du W, Yang B. Long non-coding RNAs as new regulators of cardiac electrophysiology and arrhythmias: molecular mechanisms, therapeutic implications and challenges. Pharmacol Ther 2019;203:107389.
[6] Wang K, Liu CY, Zhou LY, Wang JX, Wang M, Zhao B, et al. APF lncRNA regulates autophagy and myocardial infarction by targeting miR-188-3p. Nat Commun 2015;6(1):6779.
[7] Altmann HM, Tester DJ, Will ML, Middha S, Evans JM, Eckloff BW, et al. Homozygous/compound heterozygous triadin mutations associated with autosomal-recessive long-QT syndrome and pediatric sudden cardiac arrest: elucidation of the triadin knockout syndrome. Circulation 2015;131(23):2051–60.
[8] Wang K, Liu F, Liu CY, An T, Zhang J, Zhou LY, et al. The long noncoding RNA NRF regulates programmed necrosis and myocardial injury during ischemia and reperfusion by targeting miR-873. Cell Death Differ 2016;23(8):1394–405.
[9] Jung M, Dodsworth M, Thum T. Inflammatory cells and their non-coding RNAs as targets for treating myocardial infarction. Basic Res Cardiol 2018;114(1):4.
[10] Li D, Chen G, Yang J, Fan X, Gong Y, Xu G, et al. Transcriptome analysis reveals distinct patterns of long noncoding RNAs in heart and plasma of mice with heart failure. PLoS One 2013;8(10):e77938.
[11] Zhang Y, Jiao L, Sun L, Li Y, Gao Y, Xu C, et al. LncRNA ZFAS1 as a SERCA2a inhibitor to cause intracellular Ca^{2+} overload and contractile dysfunction in a mouse model of myocardial infarction. Circ Res 2018;122(10):1354–68.
[12] Mao Q, Liang XL, Zhang CL, Pang YH, Lu YX. LncRNA KLF3-AS1 in human mesenchymal stem cell-derived exosomes ameliorates pyroptosis of cardiomyocytes and myocardial infarction through miR-138-5p/Sirt1 axis. Stem Cell Res Ther 2019;10(1):393.
[13] Gunata M, Parlakpinar H. A review of myocardial ischaemia/reperfusion injury: pathophysiology, experimental models, biomarkers, genetics and pharmacological treatment. Cell Biochem Funct 2021;39(2):190–217.
[14] Cheng W, Wu P, Du Y, Wang Y, Zhou N, Ge Y, et al. Puerarin improves cardiac function through regulation of energy metabolism in streptozotocin–nicotinamide induced diabetic mice after myocardial infarction. Biochem Biophys Res Commun 2015;463(4):1108–14.
[15] Dai Y, Song J, Li W, Yang T, Yue X, Lin X, et al. RhoE fine-tunes inflammatory response in myocardial infarction. Circulation 2019;139(9):1185–98.
[16] Zhu SB, Xu YQ, Gao H, Deng Y. NF-κB inhibitor QNZ protects human chondrocyte degeneration by promoting glucose uptake through GLUT4 activation. Eur Rev Med Pharmacol Sci 2020;24(9):4642–51.
[17] Hou J, Wang C, Ma D, Chen Y, Jin H, An Y, et al. The cardioprotective and anxiolytic effects of Chaihujialonggumuli granule on rats with anxiety after acute myocardial infarction is partly mediated by suppression of CXCR4/NF-κB/GSDMD pathway. Biomed Pharmacother 2021;133:111015.
[18] Yin C, Ye Z, Wu J, Huang C, Pan L, Ding H, et al. Elevated Wnt2 and Wnt4 activate NF-κB signaling to promote cardiac fibrosis by cooperation of Fzd4/2 and LRP6 following myocardial infarction. EBioMedicine 2021;74:103745.

[19] Han Y, Liao X, Gao Z, Yang S, Chen C, Liu Y, et al. Cardiac troponin I exacerbates myocardial ischaemia/reperfusion injury by inducing the adhesion of monocytes to vascular endothelial cells via a TLR4/NF-κB-dependent pathway. Clin Sci 2016;130(24):2279–93.
[20] Li J, Li Y, Liu Y, Yu H, Xu N, Huang D, et al. Fibroblast growth factor 21 ameliorates NaV1.5 and Kir2.1 channel dysregulation in human AC16 cardiomyocytes. Front Pharmacol 2021;12:715466.
[21] Liang H, Pan Z, Zhao X, Liu L, Sun J, Su X, et al. LncRNA PFL contributes to cardiac fibrosis by acting as a competing endogenous RNA of let-7d. Theranostics 2018;8(4):1180–94.
[22] Zincarelli C, Soltys S, Rengo G, Rabinowitz JE. Analysis of AAV serotypes 1–9 mediated gene expression and tropism in mice after systemic injection. Mol Ther 2008;16(6):1073–80.
[23] Zhang C, Zhang L, Chen S, Feng B, Lu X, Bai Y, et al. The prevention of diabetic cardiomyopathy by non-mitogenic acidic fibroblast growth factor is probably mediated by the suppression of oxidative stress and damage. PLoS One 2013;8(12):e82287.
[24] Zhang Y, Liu X, Bai X, Lin Y, Li Z, Fu J, et al. Melatonin prevents endothelial cell pyroptosis via regulation of long noncoding RNA MEG3/miR-223/NLRP3 axis. J Pineal Res 2018;64(2):e12449.
[25] Wu X, Zhang H, Qi W, Zhang Y, Li J, Li Z, et al. Nicotine promotes atherosclerosis via ROS–NLRP3-mediated endothelial cell pyroptosis. Cell Death Dis 2018;9(2):171.
[26] Zhang Y, Li X, Zhang Q, Li J, Ju J, Du N, et al. Berberine hydrochloride prevents postsurgery intestinal adhesion and inflammation in rats. J Pharmacol Exp Ther 2014;349(3):417–26.
[27] Zhang Y, Qin W, Zhang L, Wu X, Du N, Hu Y, et al. MicroRNA-26a prevents endothelial cell apoptosis by directly targeting TRPC6 in the setting of atherosclerosis. Sci Rep 2015;5(1):9401.
[28] Li X, Yu T, Shan H, Jiang H, Sun J, Zhao X, et al. LncRNA PFAL promotes lung fibrosis through CTGF by competitively binding miR-18a. FASEB J 2018;32(10):5285–97.
[29] Del Re DP, Amgalan D, Linkermann A, Liu Q, Kitsis RN. Fundamental mechanisms of regulated cell death and implications for heart disease. Physiol Rev 2019;99(4):1765–817.
[30] Toldo S, Mauro AG, Cutter Z, Abbate A. Inflammasome, pyroptosis, and cytokines in myocardial ischemia-reperfusion injury. Am J Physiol Heart Circ Physiol 2018;315(6):H1553–68.
[31] Sun Z, Zhang L, Li L, Shao C, Liu J, Zhou M, et al. Galectin-3 mediates cardiac remodeling caused by impaired glucose and lipid metabolism through inhibiting two pathways of activating Akt. Am J Physiol Heart Circ Physiol 2021;320(1):H364–80.
[32] Wang Y, Jia L, Shen J, Wang Y, Fu Z, Su SA, et al. Cathepsin B aggravates coxsackievirus B3-induced myocarditis through activating the inflammasome and promoting pyroptosis. PLoS Pathog 2018;14(1):e1006872.
[33] Prabhu SD, Frangogiannis NG. The biological basis for cardiac repair after myocardial infarction: from inflammation to fibrosis. Circ Res 2016;119(1):91–112.
[34] Yang L, Li P, Yang W, Ruan X, Kiesewetter K, Zhu J, et al. Integrative transcriptome analyses of metabolic responses in mice define pivotal lncRNA metabolic regulators. Cell Metab 2016;24(4):627–39.
[35] Lawrence T. The nuclear factor NF-kappaB pathway in inflammation. Cold Spring Harb Perspect Biol 2009;1(6):a001651.
[36] Huxford T, Huang DB, Malek S, Ghosh G. The crystal structure of the IκBα/NF-κB complex reveals mechanisms of NF-κB inactivation. Cell 1998;95(6):759–70.
[37] Hayden MS, Ghosh S. Shared principles in NF-κB signaling. Cell 2008;132(3):344–62.
[38] Aachoui Y, Sagulenko V, Miao EA, Stacey KJ. Inflammasome-mediated pyroptotic and apoptotic cell death, and defense against infection. Curr Opin Microbiol 2013;16(3):319–26.
[39] Zhu B, Zhang L, Liang C, Liu B, Pan X, Wang Y, et al. Stem cell-derived exosomes prevent aging-induced cardiac dysfunction through a novel exosome/lncRNA MALAT1/NF-κB/TNF-α signaling pathway. Oxid Med Cell Longev 2019;2019:9739258.
[40] Mangan MSJ, Olhava EJ, Roush WR, Seidel HM, Glick GD, Latz E. Targeting the NLRP3 inflammasome in inflammatory diseases. Nat Rev Drug Discov 2018;17(8):588–606.
[41] Yu X, Lan P, Hou X, Han Q, Lu N, Li T, et al. HBV inhibits LPS-induced NLRP3 inflammasome activation and IL-1β production via suppressing the NF-κB pathway and ROS production. J Hepatol 2017;66(4):693–702.
[42] Wu X, Qian S, Zhang J, Feng J, Luo K, Sun L, et al. Lipopolysaccharide promotes metastasis via acceleration of glycolysis by the nuclear factor-κB/Snail/Hexokinase3 signaling axis in colorectal cancer. Cancer Metab 2021;9(1):23.
[43] Han B, Wang J, Wu J, Yan F, Wang Y, Li J. High glucose–induced upregulation of CD36 promotes inflammation stress via NF–κB in H9c2 cells. Mol Med Rep 2021;24(5):764.